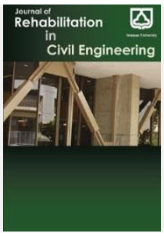

Journal of Rehabilitation in Civil Engineering

Journal homepage: https://civiljournal.semnan.ac.ir/

Assessing the Influence of Local Rebar Strain Demand on the Cyclic Behavior and Repairability of Concrete Beams Reinforced with Steel and GFRP Rebars

Amir Azarpour [1]; Saeed Tariverdilo [2,*]; Mohammad Reza Sheidaii [2]

1. Ph.D. Candidate, Department of Civil Engineering, Urmia University, Urmia, Iran
2. Professor, Faculty of Civil Engineering, Urmia University, Urmia, Iran
* Corresponding author: *s.tariverdilo@urmia.ac.ir*

ARTICLE INFO

Article history:
Received: 14 June 2024
Revised: 02 September 2024
Accepted: 07 November 2024

Keywords:
Debonding;
Plastic strain;
Repairability;
Resilience;
Seismic performance;
GFRP reinforcement.

ABSTRACT

Yielding of longitudinal rebars in reinforced concrete (RC) elements leads to the localization of damage and consequently increases repair costs. Two options are available to mitigate this localization in rebar strain: the use of debonded-steel rebars or Glass Fiber Reinforced Polymer (GFRP) rebars. An experimental program was devised, including three specimens with steel, debonded-steel, and GFRP rebars. There is a bold change in the crack pattern, from localized in the case of steel rebar with a crack width of 35 mm, to distributed cracks in the cases of debonded-steel and GFRP rebars, with a crack width smaller than 3 mm. This indicates a significant improvement in terms of repairability for these specimens. The failure drifts of the specimens are 3.5%, 3.5%, and 5.5%, respectively. Results also show that the debonding of steel rebars increases energy dissipation. This demonstrates that by following current practices in the design and construction of RC elements, and simply by debonding steel rebars, it is possible to decrease repair costs.

E-ISSN: 2345-4423

How to cite this article: Azarpour, A., Tariverdilo, S., & Sheidaii, M. (2025). Assessing the Influence of Local Rebar Strain Demand on the Cyclic Behavior and Repairability of Concrete Beams Reinforced with Steel and GFRP Rebars. Journal of Rehabilitation in Civil Engineering, 13(3), 1-21. https://doi.org/10.22075/jrce.2024.34264.2106

1. Introduction

1.1. Localization of deformations

In the engineering community, the yielding of reinforcing bars in reinforced concrete (RC) structures is generally considered a positive behavior. It places a limit on the flexural strength of RC elements, which in turn caps the demand on actions with brittle failure modes during exceptional loadings such as seismic events. However, there's a trade-off: yielding localizes deformation to specific sections. This localization results in significant strain on the rebars, and the compatibility of deformation with concrete leads to wider cracks.

Localization if comes together with softening in the response could lead to size effect, for example in the case of punching shear failure. That makes prediction of failure load a challenging issue (e.g. [1]). In fact, in RC elements one of the main aims of using rebar is to avoid localization of cracks in concrete. The same concept also applies for different measures to reinforce for example soil [2].

Indeed, the localization of yielding in reinforced concrete structures has significant implications. One direct consequence is the increased need for repair of affected elements. As localization becomes more pronounced, the level of required repair work rises, potentially compromising the overall resilience of the structure.

To control the degree of deformation localization, various design codes recommend introducing a minimum value for the ratio of the ultimate strength of the rebar (f_u) to its yield strength (f_y). For instance, in ACI 318-19 [3], this limit is expressed as f_u/f_y>1.25, and a similar criterion is adopted in AISC 341-16 [4] as f_y/f_u>0.8. By imposing this limit, the localization length increases, resulting in lower strain demands on both the rebar and the concrete. In other words, a larger modulus of elasticity for the rebar at large deformations can lead to less localized deformation. When it comes to fiber-reinforced polymer (FRP) tensile response, the absence of yielding isn't necessarily as detrimental as engineers often assume. A large modulus of elasticity for the rebar during significant deformations can mitigate localization effects and enhance the overall behavior of the structure.

There are two ways to limit this localization.

a. The first method involves debonding the rebar from the concrete. This process increases the localization length, which subsequently reduces the localized strain demand on both the concrete and the rebar. As a result, the resilience of the reinforced concrete (RC) element is enhanced. A straightforward approach to achieve this is by using a collar steel tube around the rebar at the location of the plastic hinge. Further details will be covered in subsection 1.2.
b. The second method involves adopting rebars with a large modulus of elasticity during large deformations (rebar strains above 0.002). This can be achieved by using fiber-reinforced polymers (FRPs) instead of traditional steel rebars. Further details will be discussed in subsection 1.3.

In the following subsections these methods will be discussed with greater details.

1.2. Debonding

Various researchers have explored the use of rebar restraining collars or steel tubes to prevent the buckling of longitudinal bars in reinforced concrete (RC) elements at plastic hinge locations. Ruangrassamee and Sawaroj [5] investigated the impact of steel tubes on the monotonic and cyclic response of RC columns. They observed a 17% increase in ductility and no buckling of the longitudinal bars when steel tubes were used. In another study, Mitra and Bindhu [6] explored the effect of steel tubes on the hysteretic response of short columns designed according to current state practices. They reported improvements in load-carrying capacity, energy dissipation, and stiffness degradation. Additionally, Mitra and Bindhu [7] studied the seismic response of RC columns. They found that using steel tubes with the same ductility allowed for a 33% increase in the spacing of shear reinforcement.

Besides preventing the buckling of longitudinal rebars, introducing steel tubes also results in rebar debonding. When rebars are bonded, a large portion of elongation occurs at the crack location, with minimal contribution from other sections. This localized strain leads to a significant increase in crack width, especially after rebar yielding. However, in the case of debonded rebars, elongation is uniformly distributed along the debonding length, resulting in reduced rebar strain. Debonding not only minimizes strain localization but also lowers repair costs and increases the fatigue life of rebars subjected to large inelastic demands.

In their study, Kawashima et al. [8] investigated the impact of full and partial debonding of longitudinal rebars in bridge columns subjected to cyclic lateral loads. They observed that the strain on a debonded longitudinal bar was significantly smaller than that on a standard longitudinal bar. Similarly, Aviram et al. [9] explored this concept in circular columns and found that developing a rocking response and reducing damage was challenging with short debonding lengths. Nikoukalam and Sideris [10] applied debonding to full-scale columns of special moment frames and discovered that it effectively decreased rebar strain localization.

Debonding has become a standard practice to enhance the ductility of anchor bars at the column-foundation interface, as specified by ACI 318-19 (Chapter 17). The code defines the debonding length as a stretching length, with a minimum requirement of 8 times the bar diameter.

Indeed, using steel tubes is a well-established technique for preventing buckling of longitudinal bars at plastic hinge locations in reinforced concrete (RC) elements. However, this adoption introduces debonding between the concrete and the rebar. This debonding increases the effective anchorage length and reduces the strain demand on the concrete and the rebar. Consequently, it enhances the repairability of the element and contributes to its overall resilience. Interestingly, while the anti-buckling effect of steel tubes has received significant attention, their impact on debonding remains relatively understudied.

1.3. GFRP rebars

Fiber-reinforced polymer (FRP) rebars have a lower modulus of elasticity [11] than steel rebars, resulting in larger deflections. Simultaneously, their rupture strain (typically between 0.02 and 0.03) exceeds the yield strain of steel rebars (approximately 0.002), but remains much smaller than the steel rebar's strain at ultimate strength (usually between 0.1 and 0.2) [12]. Although the elastic modulus of elasticity of steel rebars is much larger than GFRP rebars, after yielding of steel rebars it is GFRP rebars with a larger modulus of elasticity. As will be discussed in the following sections, this leads to interesting consequences.

The prime reason for using fiber-reinforced polymer (FRP) rebars instead of steel rebars is to enhance the strength and corrosion resistance of RC elements. Research [13] on the long-term field performance of glass fiber-reinforced polymer (GFRP) rebars consistently confirms their superior performance compared to steel rebars, especially in adverse environments.

Considering lack of ductility in the GFRP rebars, excluding works on the development length of these bars, research on GFRP-RC elements can be categorized into two main groups.

- Research studies that primarily focused on the strength and crack patterns of GFRP-RC elements. Habib and Ashour [14] explored the ultimate response of beams reinforced with GFRP rebars, with a particular emphasis on the impact of the amount of GFRP rebars on the overall performance. Their findings indicated that an increase in the quantity of GFRP rebars led to improved crack patterns and enhanced ultimate strength.

Nguyen et al. [15] conducted research on the crack patterns and strength of RC beams reinforced with a combination of GFRP and steel rebars (hybrid rebars). They also considered toughness in their analysis and identified an optimal percentage of rebars. Additionally, they assessed the effect of using hybrid rebars on crack patterns.

- Research efforts that focused on enhancing the ductility of GFRP-RC elements. Hadi et al. [16] conducted tests on RC columns reinforced with GFRP rebars and found that the ductility of GFRP-RC elements is comparable to that of S-RC ones. Renić and Kišiček [17] proposed a theoretical treatment to enhance ductility in FRP-RC elements by confining the concrete compression zone. Their findings indicated that confinement could significantly increase the ductility of these elements. Amirabad et al. [18] experimentally investigated the impact of confinement on the ductility of GFRP-RC elements using precast confined blocks. They observed a substantial improvement in ductility when the compression concrete was confined. Renić et al. [19] explored ductility enhancement by using hybrid rebars. Their analytical treatment highlighted that the position of FRP rebars plays a crucial role in controlling ductility. Araba and Ashour [20] experimentally studied the flexural response of beam elements reinforced with GFRP rebars, steel rebars, and hybrid rebars. They assessed the accuracy of an analytical model and code equations.

Regarding the ultimate response of RC elements with GFRP rebars, there are two points with different consequences on the ultimate response of GFRP-RC elements.

- GFRP rebars have a significantly smaller rupture strain compared to steel rebars. As a result, research in the literature has primarily focused on improving the ductility of GFRP-RC elements. Researchers have explored various methods to enhance ductility. One approach involves providing some form of confining reinforcement to the compression concrete. Through this method, they have demonstrated that the ductility of GFRP-RC elements can be comparable to that of S-RC (Steel-Reinforced Concrete) elements. Another strategy is using hybrid rebars, which combine GFRP and steel rebars.
- GFRP rebars exhibit a substantially larger modulus of elasticity at strains above 0.002 (corresponding to the yielding of steel rebars). This property results in much smaller crack widths for elements with GFRP rebars during ultimate deformations and prevents crack localization, which occurs in the case of steel rebars, especially after yielding. Consequently, repair costs for GFRP-RC elements could be reduced in the event of large displacements (deflections), such as those caused by seismic loading.

Interestingly, the superior behavior of GFRP-RC elements specifically their better resilience has not received adequate attention in the existing literature.

1.4. The need for this research

This study investigates how by mitigating local strain demand in the longitudinal rebars we could increase the repairability of reinforced concrete flexural elements. For this purpose, efficacy of: a) conventional design with steel rebars, b) conventional design with debonded-steel rebars, c) a specimen with GFRP rebars, is investigated through an experimental program.

2. The experimental program

The reduction of local strain demand in longitudinal reinforcements significantly impacts the repairability of an element after an earthquake. This study evaluates the effects of two options in achieving this reduction: the use of deboned-steel/GFRP rebars.

Considering limitations in the laboratory facility, the following factors are considered in the design of the specimens

- As discussed in the previous section, rebar buckling initiates at smaller displacements in elements with larger depth. Therefore, considering jack loading limitation, for the specimen in this study, a depth of 500 mm was chosen.
- Various modes of failure can limit the load-carrying capacity of a specimen. To ensure that rebar buckling is the dominant failure mode controlling the specimen's performance, the ratio of transverse reinforcement spacing to longitudinal bar diameter (s/d_b) was carefully selected. Specifically for specimen No. 1 and 2, the s/d_b ratio was approximately 9, and for specimen No. 3, this ratio was about 12.5. These values significantly exceed the limits typically considered for ductile flexural elements (usually set at 6). Maintaining a higher s/d_b ratio, guarantees that rebar buckling is the primary failure mechanism.

The experimental program includes three specimens:

- Specimen No. 1 (conventional design with steel rebars): This specimen is reinforced with longitudinal steel rebars, without any steel tube at the location of plastic hinge, representing conventional design adopting current state of practice. The steel bar diameter is 12 mm, and the resulting s/d_b is about 9.
- Specimen No. 2 (conventional design with debonded-steel rebars): This is the same as specimen 1, however it has steel tube at the location of plastic hinge.
- Specimen No. 3 (specimen with GFRP rebars): This specimen has the same dimension as that of specimen 1, however its longitudinal rebars are GFRP bars with bar diameter of 8.5 mm. The resulting s/d_b for this specimen is about 12.5 that is much larger of the value for the specimen No. 1 and 2.

Table 1 gives the material properties of the steel/GFRP rebars, and concrete. Maximum aggregate size is 25 mm and fineness modulus for sand and gravel is 2.9 and 6.8, respectively. The specimens are blanket-cured for 7 days. Cement, sand and coarse aggregate are used in the ratio of 1:2.5:3.3, and water cement ratio is limited to 0.35.

Table 1. Steel and GFRP material properties.

Material	Material Property		MPa/%	Unit
Steel Rebar	Yield stress		488	MPa
	Yield strain		0.0024	%
	Ultimate stength		625	MPa
	Fracture elongation measured on	$5d_b$	0.29	%
		$10d_b$	0.26	%
		200 mm	0.21	%
GFRP	Ultimate stress		996	MPa
	Rupture strain		0.024	%
Steel Tube	Yield stress		457	MPa
Concrete	28 days compressive strength		25	MPa
	Modulus of elasticity		28500	MPa

The considerations for determining the required length of the steel tube includes:

- **Stretching length requirement (ACI 318-19):** According to ACI 318-19, the length of the steel tube should be at least 8 times the diameter of the rebar.

- **Plastic hinge length:** The steel tube length should be at least equal to the plastic hinge length. In this case, the plastic hinge length of the specimen is approximately 250 mm.
- **Buckling considerations:** Considering that the buckling length of the rebar could exceed the spacing of the transverse reinforcements, it's common practice to use a steel tube length approximately two times the spacing of the transverse reinforcements. This results in a minimum steel tube length of about 220 mm.

Steel tube used in this study has length of 300 mm, with inner and outer diameters of 16.7 and 21.3 mm, respectively. It's yield stress is reported in Table 1.

To assess the impact of reinforcement type on the seismic performance of the specimen, the third specimen incorporates longitudinal GFRP rebars. These rebars have limited deformation capacity but significantly higher uniaxial strength. Unlike steel rebars, the GFRP rebar exhibits limited tensile strain before rebar failure. Compared with the specimen No. 1 and 2, specimen No. 3 will show the adverse effects of cyclic yielding.

The test setup, which includes a stub column, is based on the work by Panagiotou et al. [21]. This setup is primarily used to evaluate the potential for rebar buckling in large reinforced concrete (RC) special moment frame beams. The dimensions and reinforcement of the stub column are carefully designed to ensure that nonlinear deformation occurs exclusively in the beams and at their juncture with the stub column. No nonlinear deformation takes place within the stub column itself. The boundary condition for the beams is simply supported, preventing any vertical movement at the supports.

Tests are carried out at the infrastructure research center of the Urmia University using a universal jack of 1000 kN capacity.

Fig. 1 presents photographs of the specimen reinforcement and a specimen positioned in the testing setup, accompanied by a schematic view of the test configuration. Specifically, Fig. 1(a) shows the installation of a steel tube on the longitudinal rebars at the juncture of the beam and stub column. Fig. 1(b) shows the rebar cage before concrete placement. Fig. 1(c) depicts the specimen placed within the test setup.

Additionally, Fig. 2) provides further insight into the specimen's schematic view and reinforcement.

The loading protocol was developed to meet the requirements outlined in ACI 374.2R [22] for cyclic tests on structural elements simulating seismic loading (see Fig.3). To account for the degrading response of the specimens and in alignment with ACI 374.2R recommendations for degrading elements, we modified the loading protocol. Instead of using two cycles for each increment, we now employ three cycles for each deformation cycle.

(a)

(b)

(c)

Fig. 1. The specimens, a) rebar cage with steel tube, b) the complete rebar cage, c) the specimen place in the test setup.

3. Experimental results

In this section, first, we will present and discuss the experimental results for each specimen. Finally, we will compare the results of all the specimens to assess the effect of debonding and rebar type. It is important to note that due to the weight of the specimen, the hysteretic response is asymmetric.

The loading protocol was developed to meet the requirements outlined in ACI 374.2R [22] for cyclic tests on structural elements simulating seismic loading (see Fig.3). To account for the degrading response of the specimens and in alignment with ACI 374.2R recommendations for degrading elements, we modified the loading protocol. Instead of using two cycles for each increment, we now employ three cycles for each deformation cycle.

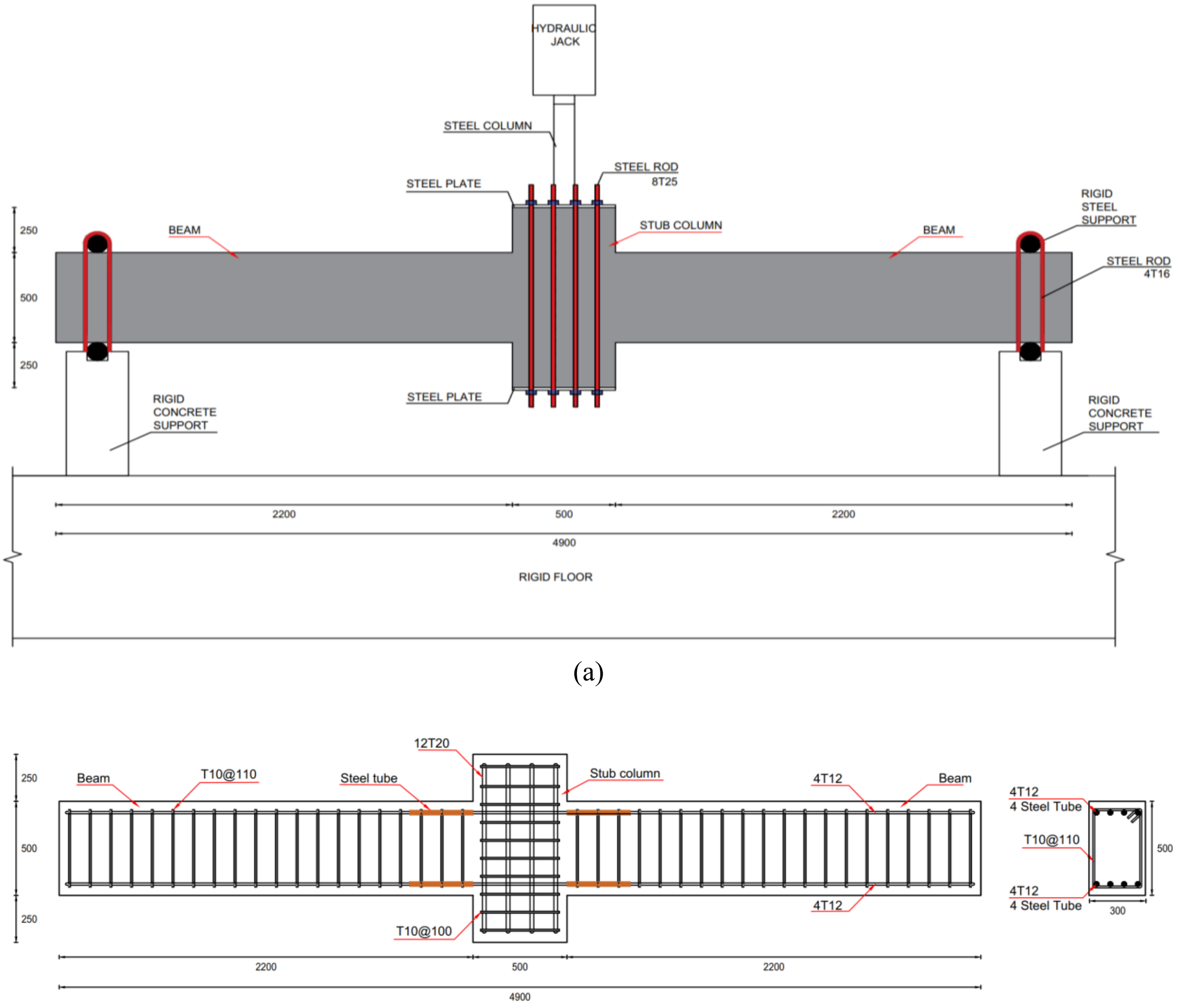

Fig. 2. The specimens, a) Schematic view, b) Reinforcing details of the specimens (all dimensions and bar diameter and spacing in mm).

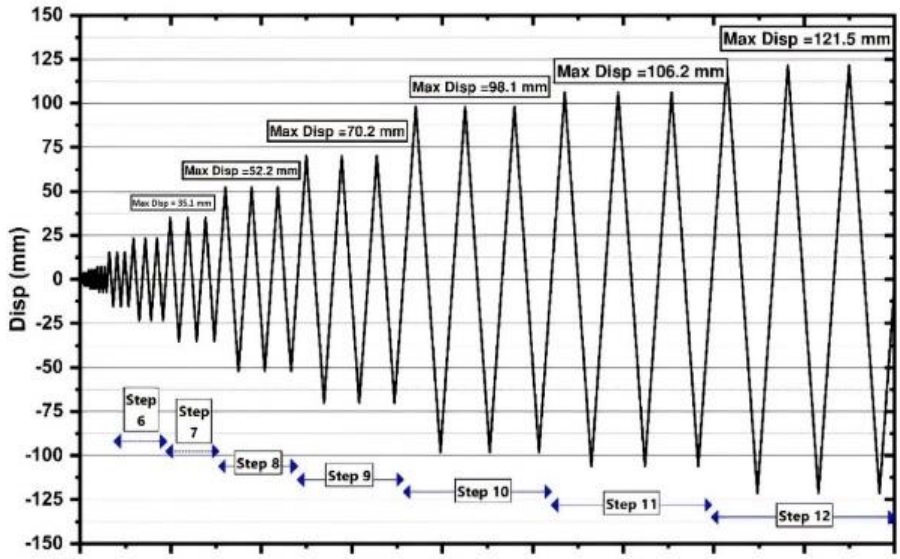

Fig.3. Loading protocol used in the experiments.

3.1. Specimen No.1: conventional design with steel rebars

The specimen has steel longitudinal rebars, without steel tube. The s/d_b ratio for the transverse reinforcement at the plastic hinge location is about 9, well above code requirements for ductile flexural elements. Considering Fig. 4, which shows the hysteretic response of the specimen, the main observations could be listed as follows:

- The maximum positive (point A) and negative (point B) displacements are about 70 mm, corresponding to 3.5% drift. Between these displacements the hysteretic response is stable, with small pinching effect due to crack closure in the reloading regions.
- By averaging maximum resisting moments in the positive and negative direction, it is possible to remove the effect of specimen weight. The resulting average moment at the beam section at the stub column interface is about 10 kN.m. The corresponding moment at the beam and stub column juncture will be about 9 kN.m. Considering the material properties of Table 1, the beam section flexural capacity is 9.5 kN.m. This agrees with the average flexure moment capacity observed in the test.
- At the end of the ninth load cycle (displacement of 70 mm, i.e., drift of 3%), buckling of the longitudinal initiates (Fig. 5 and Fig. 6(a) and Fig. 6(b). this triggers substantial strength degradation in the subsequent loading steps. As could be seen, at this load step the slop of the load-deflection diagram becomes negative. In other words, there is softening in the response. It is well known that in the case of softening (or in-cycle strength degradation [23]) damage localizes on some sections, and this is a good example this localization.
- Damage localization as could be seen in Fig. **5** of the paper, when the cracks on either side of the damaged section reaches together could trigger sliding shear failure. Also, it is widely recognized that damage localization could lead to rebar fracture or at much lower strains low cycle fatigue failure of the rebar.
- Significant loss of strength starts at tenth cycle of loading at point C. Points D, E and F depicts consecutive fracture of first, second and third longitudinal rebars in the top side of beam (Fig. 6(c)), that occurs at tenth step of loading protocol. At point F the test is terminated.
- The yield displacement of the specimen is about 14 mm. Therefore, the displacement ductility of the specimen is about 5. This corresponds to a drift of about 3.5%.

Specimen No. 1 experienced complete failure after 2 hours and 37 minutes, at the end of the first cycle of the tenth loading step.

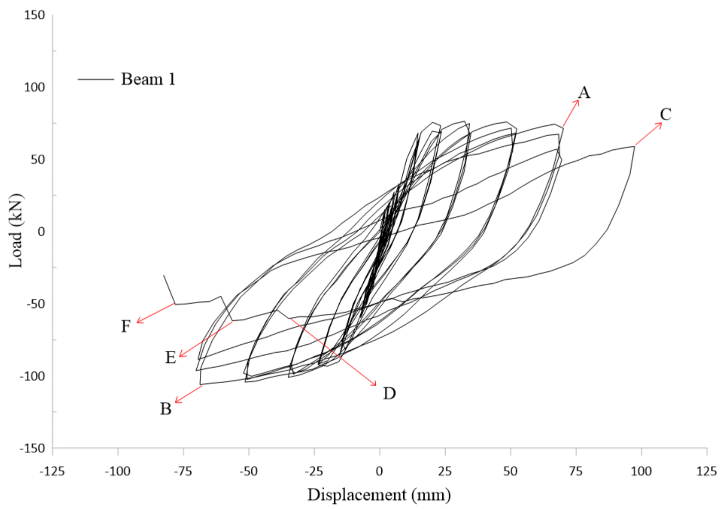

Fig. 4. Hysteresis response of specimen No. 1.

Fig. 5. Specimen No. 1 at the end of cycle 9, with a displacement of 70 mm (drift of 3.5%).

(a)

(b)

(c)

Fig. 6. State of specimen No. 1 at different stages of test: a) buckling of bottom reinforcement, b) buckling of top reinforcements, c) fracture of longitudinal rebars.

3.2. Specimen No. 2: conventional design with debonded-steel rebars

This specimen is the same as specimen No. 1, but there are collar steel tubes around steel rebars. These steel tubes debonding the rebars from concrete also enhance the buckling resistance of the longitudinal bars. Considering the hysteretic response of the specimen (Fig. 7), the main observations are:

- The maximum positive (point A) and negative (point B) displacements are about 98 and 70 mm (drift of 4.9% and 3.5%), respectively. This shows slightly larger maximum displacements for the positive displacements than the specimen No. 1.
- Slight but not meaningful increase in the strength could be observed for this specimen compared to the specimen No. 1.
- Significant degradation in the response starts at the end of ninth load cycle at the same displacement observed for the specimen No. 1. This is mainly due to start of rebar buckling as could be seen in Fig. 9. As can be observed in this figure buckling starts at the stub column cover. It suggests that we could expect further improvement in the response if the steel tube penetrates the column cover rather than terminating at the column face.
- Fracture of the longitudinal bars due to low cycle fatigue starts at the second cycle of the tenth load step. Points D, E and F depicts consecutive fracture of first, second and third longitudinal rebars in the top side of beam (Fig. 9), and points G, H and I denotes the same points for rebars on the opposite side of the beam.
- Comparing the pattern of cracks at displacement of 70 mm (drift of 3.5%) in Fig. 5 and Fig. 8, significant localization of deformation could be observed for the specimen No. 1 compared to the specimen No. 2. These could be attributed to anti-buckling and debonding actions of steel tube.
- Considering yield displacement of 14 mm, the positive and negative displacement ductility of the specimen are about 7 and 5. A slight increase in the displacement ductility for the positive direction could be noted.
- At the end of test, except cover spalling there is no significant crack at the beam in the plastic hinge region (Fig. 10).

Failure of specimen No. 2 occurred in the plastic hinge zone, after 2 hours and 52 minutes, in the second cycle of the tenth loading step.

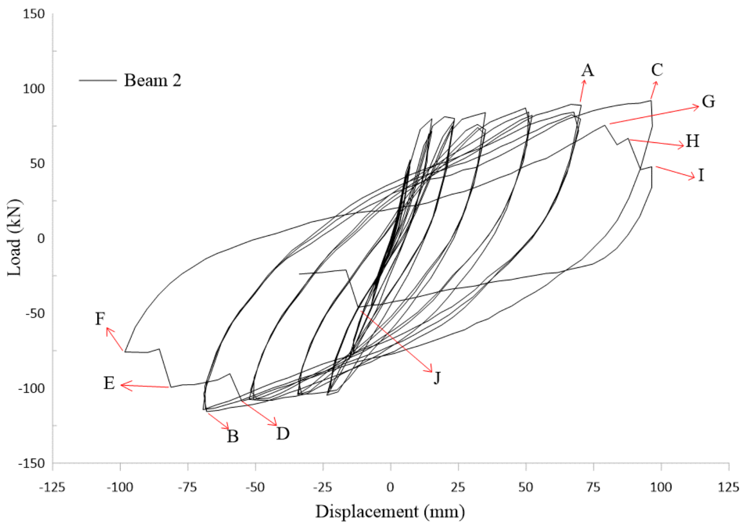

Fig. 7. Hysteresis response of specimen No. 2.

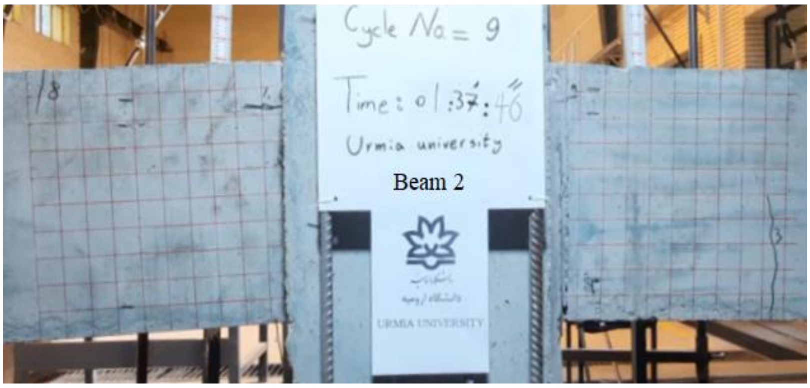

Fig. 8. State of specimen No. 2 at the end of load cycle 9 with a displacement of 70 mm (drift of 3.5%).

Fig. 9. Buckling state of the longitudinal rebar in specimen No. 2 with steel tube. Note that the rebar buckling start in the cover of stub column.

Fig. 10. State of the specimen No. 2 at the end of the test.

3.3. Specimen No. 3: Specimen with GFRP rebars

In specimen No. 3, the GFRP rebars have been substituted with steel ones. While the diameter of the steel rebars in specimens No. 1 and 2 is 12 mm, the diameter of GFRP rebars is only 8.5 mm. This leads to a much larger s/d_b ratio for this specimen (about 12.5). The main observations regarding the performance of this specimen, considering Fig. 11, are

- The maximum resistance of beam 3 in the positive direction of loading is 100 kN, which occurred at a displacement of 106 mm (point E corresponding to 5.3% drift). Also, in the negative direction of loading, the maximum resistance is 136 kN, which occurs in the displacement of 122 mm and drift of 6.1% (point H).
- At the first cycle of the 12^{th} step, a fracture of one of the longitudinal reinforcements happens (point G). The experiment was terminated due to the failure of one more reinforcement in the third cycle of the 12^{th} step (point J).
- Even at much larger displacements, compared to the specimen No. 1 and 2, the extent of damage and crack width are much smaller (Fig. 12 and Fig. 13).
- While there is no significant increase in the strength, a substantial increase in the maximum displacement and ductility of the specimen compared to that observed for the specimen No. 1 and 2 is observed. At the same time, there is significant pinching in the hysteretic response, which means less desirable energy dissipation behavior.
- The specimen can withstand drifts as much as 6.1%.

Failure of specimen No. 3 with GFRP reinforcements occurred after 5 hours and 31 minutes, in the third cycle of the 12^{th} loading step.

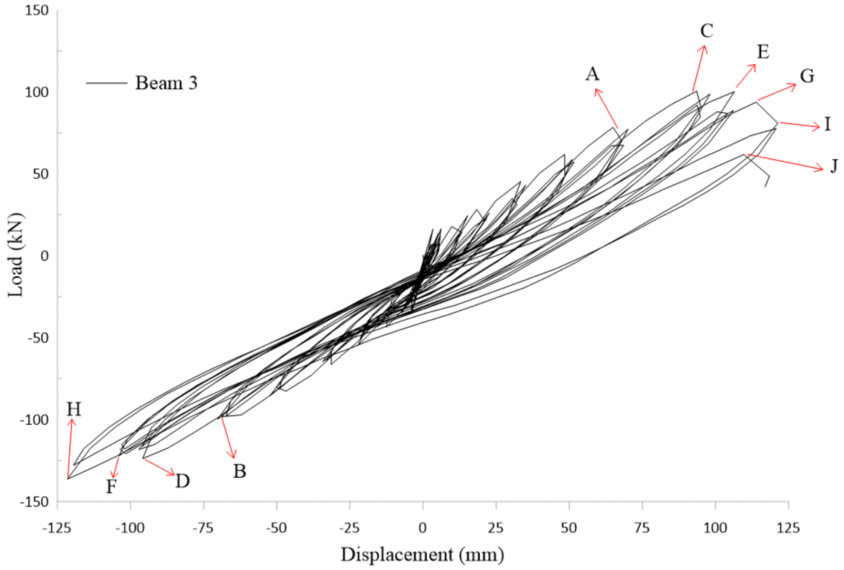

Fig. 11. Hysteresis response of specimen No. 3.

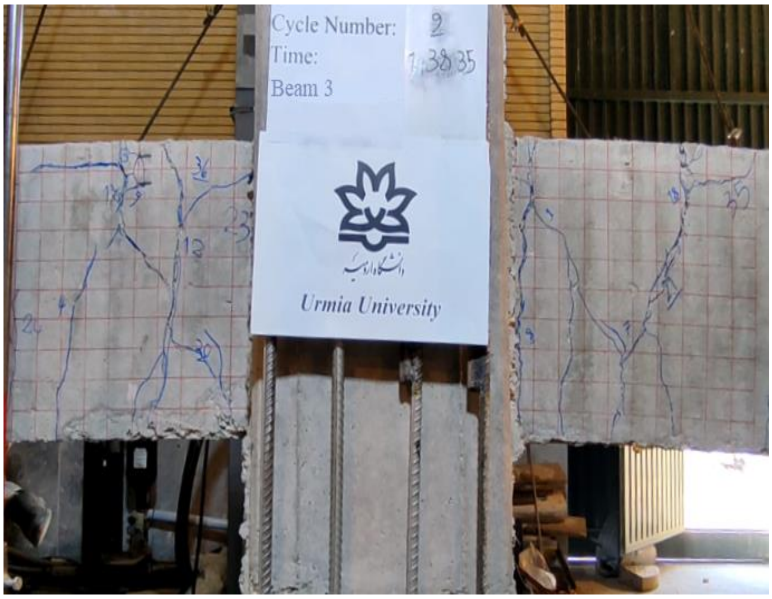

(a)

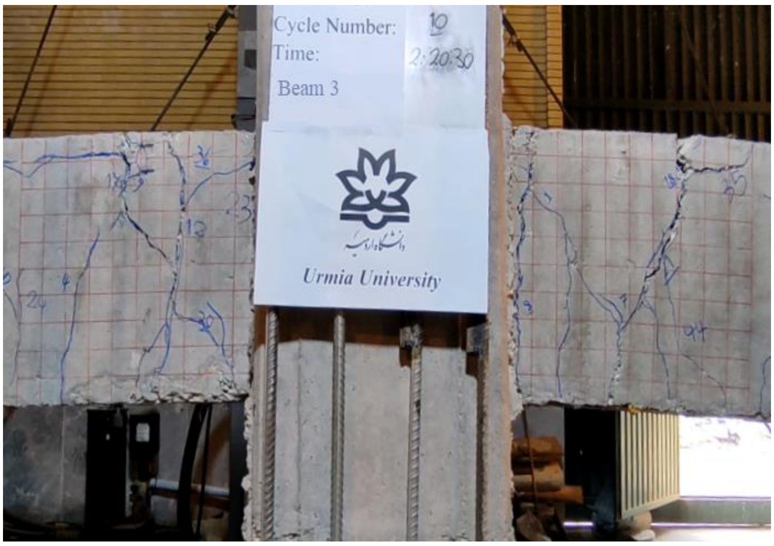

(b)

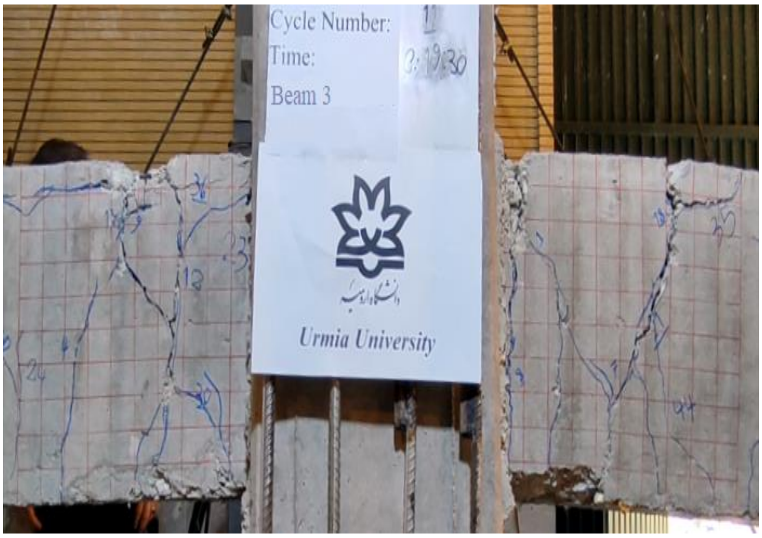

(c)

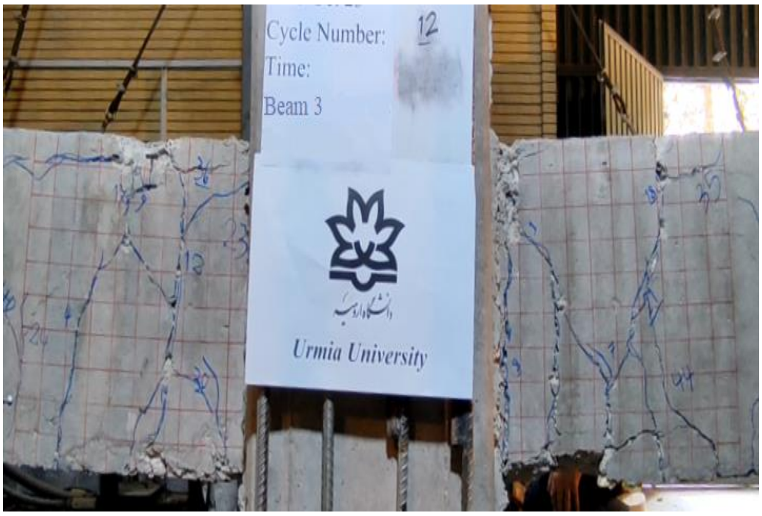

(d)

Fig. 12. State of the specimen No. 3, a) at displacement of 70 mm (drift of 3.5%), b) at displacement of 98 (drift of 4.9%), c) at displacement of 106 (drift of 5.3%), d) at displacement of 122 mm (drift of 6.1%).

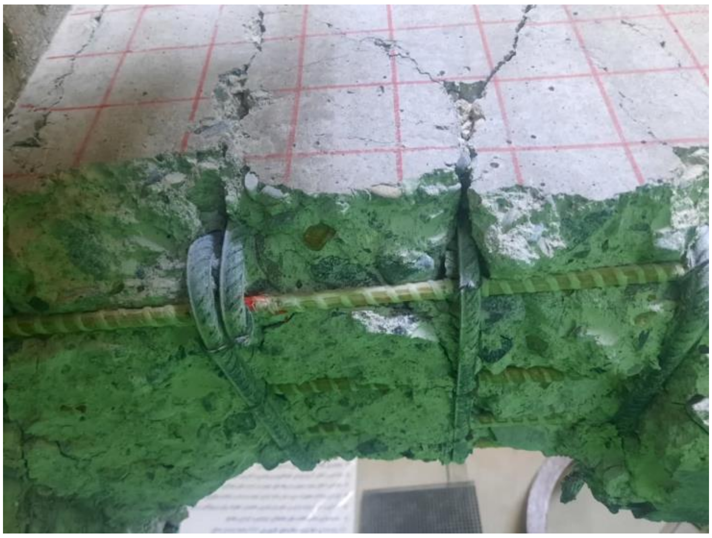

Fig. 13. Closer look at the damaged state of the specimen No. 3 in the plastic hinge region.

3.4. Comparison of the behavior of the specimens

Fig. 14 presents a pairwise comparison of the hysteretic response of three specimens. Table 2 compares the performance of the specimens. The moment capacity of specimens with steel/GFRP rebars was calculated based on ACI 318-19/ACI 440.1R-15 [24]. Notably, there is a good correlation between experimental results and code predictions.

Additionally in Table 2, the rebar strain at the start of rebar buckling was evaluated. For specimens No. 1 and 2, rebar buckling occurs at a drift of 3.5%. We compared this rebar strain with the predictions from Rodriguez et al.'s model [25] for rebar buckling, assuming a double modulus with an effective length factor of 0.75 and s/d_b=9. Remarkably, there is excellent agreement in this regard.

Extending the applicability of the Rodriguez model to specimens with GFRP rebars, the best prediction of the model for rebar strain at the initiation of rebar buckling (for s/d_b=12.5) is 0.01. Interestingly, no rebar buckling is observed in this specimen, highlighting another beneficial effect of GFRP rebars, which is their large modulus of elasticity at large strains.

Finally, the damage state of the specimens at a drift of 3.5% was compared. Specimen No. 1 exhibited the worst performance, while specimen No. 2 performed the best.

Table 2. Comparing experimental results with code predictions and evaluating strain and damage state at drift of 3.5%.

specimen	Moment capacity (kN.m)		Assumed plastic hinge length (mm)	State at drift of 3.5%				Cause of failure
	Experiment	ACI 318-19/ACI 440.1R-15		Calculated rebar strain	Buckling strain based on Rodriguez et al. model	Max. crack width (mm)	Damage state	
1	9.0	9.5	250	0.035	0.032	35	poor	Rebar buckling
2	9.0	9.5	300	0.029	0.032	1	good	Rebar buckling
3	9.0	8.8	300	0.029	0.01	3	acceptable	Rebar rupture

The following points could be drawn from these comparisons:

- Although specimen No. 1 and 2 have the same maximum displacement capacity, specimen No. 2 has much better energy dissipation with a much smaller pinching effect (Fig. 14(a)).
- Noting that the only difference between the specimen No. 1 and 2 is the use of steel tube in the latter one, at same displacement demand (120 mm) the damage extent in the specimen No. 2 is much less than that for the specimen No. 1 (comparing Fig. 5 and Fig. 8). This also means better repairability and resilience of the specimen No. 2.
- As seen in Fig. 9, buckling of the steel rebars in the specimen No. 2 starts at spalled cover of the stub column. It is anticipated that further improvement in the response of the specimen No. 2 could be provided if the steel tube terminated not at the stub column face but at its core interface.

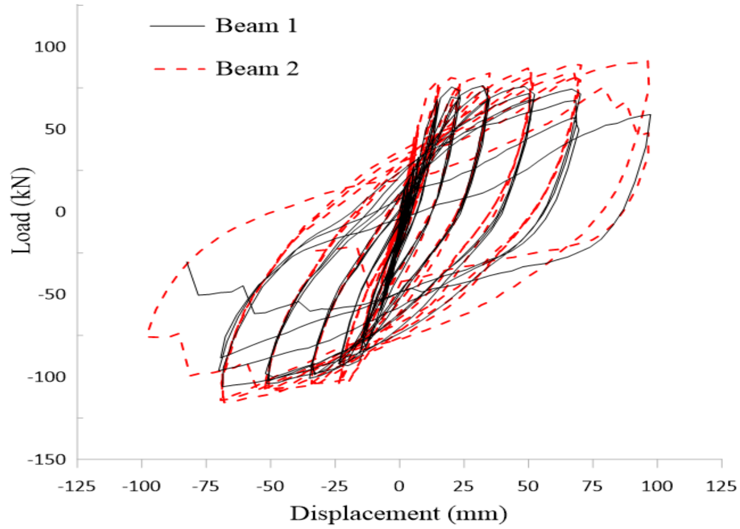

(a)

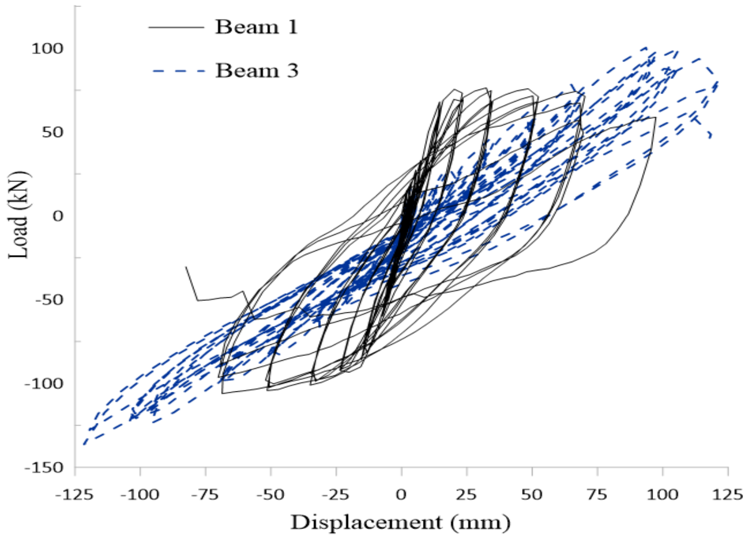

(b)

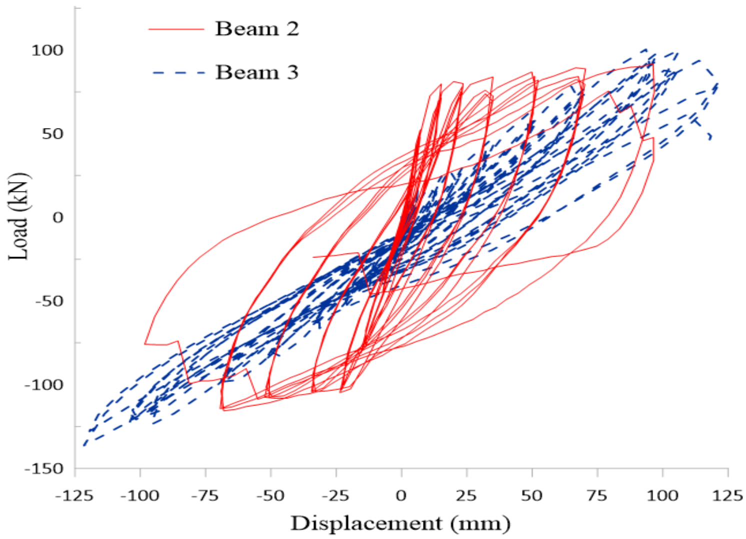

(c)

Fig. 14. Comparison of different specimens: a) specimen No. 1 versus 2, b) specimen No. 1 versus 3, c) specimen No. 2 versus 3.

- It is well known that rebar buckling is related to the maximum plastic strain experienced by the rebar. In the case of the specimen No. 2, it seems that debonding action of the steel tube by reducing local strain demand on the longitudinal rebars reduces the probability of buckling and increases fatigue life of the rebar.
- Comparing specimens No. 1 and 3 shows the adverse effect of the rebar plastic strain on the rebar buckling (Fig. 14(b)). While s/d_b for these specimens are 9 and 12.5, respectively, specimen No. 3 could withstand much larger displacements, with no rebar buckling.
- The energy dissipation of specimen No. 3 compared to the other specimens is poor and shows significant pinching.
- Specimen No. 2 exhibits the best performance, featuring favorable energy dissipation characteristics and a damage pattern that facilitates effective repairability.

4. Conclusions

This study investigates the importance of mitigating local longitudinal rebar strain on the energy dissipation and repairability of concrete beams reinforced by steel or GFRP rebars. To this end, three specimens were experimentally tested. The first one is an ordinary reinforced concrete beam with steel rebars (conventional design). In the second test steel tubes are place around the longitudinal bars at the location of plastic hinges (debonded conventional design). The final test employs GFRP rebars rather than steel ones. The following conclusions could be drawn from this set of experiments.

4.1. Crack width and repairability

When comparing the performance of different specimens at a drift of 3.5%, it can be concluded that employing debonded-steel/GFRP rebars significantly leads to a distributed pattern of small cracks. In conventional designs, there is a localized crack with a width of 35 mm, but in the debonded-steel/GFRP specimens, there is a pattern of distributed cracks with a width of at most 3 mm. This indicates that using debonded-steel/GFRP rebars can significantly reduce the need for repairs in elements with significant plastic hinge rotation.

4.2. Localization effect on rebar buckling

The prediction of rebar buckling by the Rodriguez et al. model at a drift of 3.5% for specimens with conventional design and debonded-steel rebar aligns precisely with the experiment. Extending the application of the Rodriguez model to the specimen with GFRP rebars predicts rebar buckling at much smaller drifts (due to the larger s/d_b ratio), while in the experiment, no rebar buckling occurs for this specimen. This could be attributed to the larger modulus of elasticity for GFRP rebars at large strains.

4.3. Failure mode and energy dissipation

While rebar buckling leads to the failure of specimens with steel rebar at a drift of 3.5%, rebar rupture is the cause of failure for the specimen with GFRP rebar at a much larger drift of 5.5%. Compared with the specimen with conventional design, there is an increase in energy dissipation for the specimen with debonded-steel rebars at large drifts. The energy dissipation of the specimen with GFRP rebars is lower compared to those with steel rebars. No dissipation occurs in GFRP rebars, and on the other hand, there is no energy dissipation in compression concrete.

4.4. Application in practice

The usual way to improve repairability is by designing for a larger base shear or smaller lateral drift. However, the results of these tests show that by following the current state of practice and simply inserting a collar steel tube, it is possible to improve the repairability and resilience of RC elements.

4.5. Misjudgment about GFRP rebars

Due to the lack of yielding in the behavior of GFRP rebars, the engineering community commonly concludes that they are unsuitable for seismic design. This study shows that the larger modulus of elasticity of GFRP rebars at large strains prevents the localization of cracks, which is the main reason for rebar buckling. On the other hand, researchers have shown that to provide better energy dissipation in RC elements with GFRP rebars; options include confining concrete and using hybrid rebars. This shows that RC elements with GFRP rebars could be used for seismic design in the near future.

Funding

This research did not receive any specific grant from funding agencies in the public, commercial, or not-for-profit sectors.

Conflicts of interest

The authors declare that they have no known competing financial interests or personal relationships that could have appeared to influence the work reported in this paper.

Authors contribution statement

Amir Azarpour: Conceptualization, Methodology, Data curation, Project administration, Writing - original draft, Writing - review & editing.

Saeed Tariverdilo: Supervision, Conceptualization, Data curation, Design, Formal analysis, Writing - original draft, Writing - review & editing.

Mohammad Reza Sheidaii: Supervision, Conceptualization, Writing - review & editing.

Acknowledgment

The authors gratefully acknowledge collaboration of Mr. Omili during test program.

References

[1] Barkhordari MS, Fattahi H, Armaghani DJ, Khan NM, Afrazi M, Asteris PG. Failure mode identification in reinforced concrete flat slabs using advanced ensemble neural networks. Multiscale Multidiscip Model Exp Des 2024. https://doi.org/10.1007/s41939-024-00554-9.

[2] Fareghian M, Afrazi M, Fakhimi A. Soil Reinforcement by Waste Tire Textile Fibers: Small-Scale Experimental Tests. J Mater Civ Eng 2023;35:4022402. https://doi.org/10.1061/(asce)mt.1943-5533.0004574.

[3] ACI 318-89. Building Code Requirements for Structural Concrete. vol. 2007. 1989.

[4] Prinz GS, Richards PW. Experimental Evaluation and Design Procedure for All-Steel Tube-in-Tube Buckling Restrained Braces. J Struct Eng 2024;150:1–15. https://doi.org/10.1061/jsendh.steng-12566.

[5] Ruangrassamee A, Sawaroj A. Seismic enhancement of reinforced-concrete columns by rebar-restraining collars. J Earthq Tsunami 2012;6:1250015. https://doi.org/10.1142/S1793431112500157.

[6] Mitra DC, Bindhu KR. Seismic performance of RC short columns with buckling restraint reinforcement. Mag Concr Res 2019;71:163–74. https://doi.org/10.1680/jmacr.17.00322.

[7] Damodaran Chitra M, Rugmini BK. Influence of Buckling Restrained Reinforcement on Behavior of Columns. Pract Period Struct Des Constr 2020;25:4020034. https://doi.org/10.1061/(asce)sc.1943-5576.0000520.

[8] KAWASHIMA K, HOSOIRI K, SHOJI G, SAKAI J. Effect of Unbonding of Main Reinforcements At Plastic Hinge Region for Enhancing Ductility of Reinforced Concrete Bridge Columns. Doboku Gakkai Ronbunshu 2001;2001:45–64. https://doi.org/10.2208/jscej.2001.689_45.

[9] Aviram A, Stojadinovic B, Parra-Montesinos GJ. High-performance fiber-reinforced concrete bridge columns under bidirectional cyclic loading. ACI Struct J 2014;111:303–12. https://doi.org/10.14359/51686522.

[10] Nikoukalam MT, Sideris P. Experimental Performance Assessment of Nearly Full-Scale Reinforced Concrete Columns with Partially Debonded Longitudinal Reinforcement. J Struct Eng 2017;143:4016218. https://doi.org/10.1061/(asce)st.1943-541x.0001708.

[11] Doost Mohamadi A, Vatani Oskouei A, Kheyroddin A. An experimental study on effect of concrete type on bond strength of GFRP bars. J Rehabil Civ Eng 2021;9:52–70. https://doi.org/10.22075/JRCE.2020.19922.1392.

[12] Kinjawadekar TA, Nagarajan P, Shashikala AP, others. Design of Short Columns Reinforced with GFRP Bars Subjected to Axial Loading. IOP Conf. Ser. Mater. Sci. Eng., vol. 936, 2020, p. 12003. https://doi.org/10.1088/1757-899x/936/1/012003.

[13] Gooranorimi O, Nanni A. GFRP Reinforcement in Concrete after 15 Years of Service. J Compos Constr 2017;21:4017024. https://doi.org/10.1061/(asce)cc.1943-5614.0000806.

[14] Habeeb MN, Ashour AF. Flexural behavior of continuous GFRP reinforced concrete beams. J Compos Constr 2008;12:115–24. https://doi.org/10.1061/(ASCE)1090-0268(2008)12:2(115).

[15] Nguyen PD, Dang VH, Vu NA. Performance of concrete beams reinforced with various ratios of hybrid GFRP/steel bars. Civ Eng J 2020;6:1652–69. https://doi.org/10.28991/cej-2020-03091572.

[16] Hadi MNS, Karim H, Sheikh MN. Experimental Investigations on Circular Concrete Columns Reinforced with GFRP Bars and Helices under Different Loading Conditions. J Compos Constr 2016;20:4016009. https://doi.org/10.1061/(asce)cc.1943-5614.0000670.

[17] Renić T, Kišiček T. Ductility of concrete beams reinforced with frp rebars. Buildings 2021;11:424. https://doi.org/10.3390/buildings11090424.

[18] Amirabad NG, Alaee FJ, Jalali M. Ductility improvement of GFRP-RC beams using precast confined concrete block in compression zone. Front Struct Civ Eng 2023;17:1585–98. https://doi.org/10.1007/s11709-023-0968-8.

[19] Renić T, Hafner I, Kišiček T. Ductility of hybrid FRP – steel reinforced concrete sections. In: Šajna A, Legat A, Jordan S, Horvat P, Kemperle E, Dolenc S, et al., editors. Proc. 2nd Int. Conf. CoMS 2020/21, 2021, p. 118–26.

[20] Araba AM, Ashour AF. Flexural performance of hybrid GFRP-Steel reinforced concrete continuous beams. Compos Part B Eng 2018;154:321–36. https://doi.org/10.1016/j.compositesb.2018.08.077.

[21] Visnjic T, Antonellis G, Panagiotou M, Moehle JP. Effects of Hoop Spacing on Seismic Performance of Large Reinforced Concrete Special Moment Resisting Frame Beams. vol. 2013. Pacific Earthquake Engineering Research Center; 2013.

[22] ACI PRC-374.2-13. Guide for Testing Reinforced Concrete Structural Elements Under Slowly Applied Simulated Seismic Loads. Am. Concr. Inst., 2013.

[23] Department of Homeland Security. FEMA 440: Improvement of nonlinear static seismic analysis procedures. Fed Emerg Manag Agency 2005;7:1–426.

[24] Busel JP, Bank LC, Brown VL, Campbell TI, Fam AZ, Lee MW. Guide for the Design and Construction of Structural Concrete Reinforced with FRP Bars Reported by ACI Committee 440. 2006.

[25] Rodriguez ME, Botero JC, Villa J. Cyclic Stress-Strain Behavior of Reinforcing Steel Including Effect of Buckling. J Struct Eng 1999;125:605–12. https://doi.org/10.1061/(asce)0733-9445(1999)125:6(605).